Journal of Biomolecular NMR, **14:** 13–22, 1999.
KLUWER/ESCOM

Separating the contributions to ^{15}N transverse relaxation in a fibronectin type III domain

Alison E. Meekhof & Stefan M.V. Freund*
MRC Unit for Protein Function and Design, University Chemical Laboratory, Lensfield Road, Cambridge CB2 1EW, U.K.

Received 16 December 1998; Accepted 18 February 1999

Key words: backbone dynamics, chemical exchange, diffusion anisotropy, fibronectin type III domain, β-sandwich protein

Abstract

In proteins, dynamic mobility is an important feature of structure, stability, and biomolecular recognition. Uniquely sensitive to motion throughout the milli- to picosecond range, rates of transverse relaxation, R_2, are commonly obtained for the characterization of chemical exchange, and the construction of motional models that attempt to separate overall and internal mobility. We have performed an in-depth study of transverse relaxation rates of backbone ^{15}N nuclei in TNfn3$_{1-90}$, the third fibronectin type III domain from human tenascin. By combining the results of spin-echo (CPMG) and off-resonance $T_{1\rho}$ experiments, we present R_2 rates at effective field strengths of 2 to 40 krad/s, obtaining a full spectrum of 16 independent R_2 data points for most residues. Collecting such a large number of replicate measurements provides insight into intrinsic uncertainties. The median standard deviation in R_2 for non-exchanging residues is 0.31, indicating that isolated measurements may not be sufficiently accurate for a precise interpretation of motional models. Chemical exchange events on a timescale of 570 μs were observed in a cluster of residues at the C terminus. Rates of exchange for five other residues were faster than the sampled range of frequencies and could not be determined. Averaged 'exchange free' transverse relaxation rates, R_2^0, were used to calculate the diffusion tensor for rotational motion. Despite a highly asymmetric moment of inertia, the narrow angular dispersion of N-H vectors within the β sandwich proves insufficient to define deviations from isotropic rotation. Loop residues provide exclusive evidence for axially symmetric diffusion ($D_{par}/D_{per} = 1.55$).

Abbreviations: TNfn3, third fibronectin type III domain from human tenascin; CPMG, Carr–Purcell–Meiboom–Gill; CSA, chemical shift anisotropy; R_2, transverse (spin-spin) relaxation rate; R_1, longitudinal (spin-lattice) relaxation rate; $R_{1\rho}$, rotating frame relaxation rate; R_{ex}, chemical exchange contribution to R_2 in Hz; τ_{ex}, chemical exchange time constant; R_2^0, 'exchange free' transverse relaxation rate; ω_{eff}, effective strength of the applied B_1 field; Δ, offset between the applied B_1 field and ^{15}N resonances; θ, offset angle between the z-axis and the effective spin lock field; θ_{N-H}, tilt angle between an N-H vector and the major diffusion axis; $\tau_{c,eff}$, effective correlation time.

Introduction

Detecting and manipulating transverse relaxation (R_2) is a fundamental aspect of NMR spectroscopy, with a wide variety of applications. The CPMG spin-echo sequence was first introduced in the 1950s to suppress transverse relaxation caused by magnetic field inhomogeneities (Carr and Purcell, 1954). Recently, the TROSY approach for attenuating R_2 has provided a key to determining NMR solution structures for very large proteins (Pervushin et al., 1997). The study of dynamic motion in proteins, often necessary for a complete understanding of stability, structure, and function (Kay, 1998), relies upon the accurate deter-

*To whom correspondence should be addressed. E-mail: smvf100@cus.cam.ac.uk

mination and interpretation of R_2. This is not always a straightforward task.

The primary mechanism for ^{15}N relaxation in proteins is the fluctuation of ^{1}H-^{15}N bond dipoles and ^{15}N CSA tensors with respect to the static magnetic field. These fluctuations result from overall tumbling of the protein (on the ns timescale) and faster, uncorrelated motions such as the floppiness of a long loop. When tumbling is not isotropic, these reorientational events do not occur with equal probability for all N-H bond vectors, and rates of relaxation depend on the polar angle between the N-H vector and the major diffusion axis, θ_{N-H}. Motion on the ms to μs timescale (chemical exchange), though less common, can exert a dramatic influence on R_2. The ms to μs interconversion of a nucleus between two or more states with different chemical shifts promotes transverse relaxation through the loss of spin coherence in the xy-plane. Separating the contributions to ^{15}N transverse relaxation is desirable, for each provides a unique insight into protein structure and mobility.

An increasing number of studies have related protein mobility to biological function (Palmer, 1997; Kay, 1998). Slower than correlated rates of overall rotation, motion on the ms to μs timescale has stirred particular interest. Such motion can result from the relative movement of secondary structural elements (hinge or shear motions), disulfide bond isomerization, and restricted side-chain rotation (Lane and Lefévre, 1994). Exchange has been detected within DNA and protein receptor binding sites (Ogata et al., 1996; Wyss et al., 1997; McIntosh et al., 1998; Whittaker et al., 1998), where the degree of motion may play a role in ligand selectivity (Constantine et al., 1998). In protein denatured states, motion on the ms to μs timescale is much slower than usual rates of conformational interconversion. It suggests the presence of relatively persistent interactions that may lead to the formation of folding initiation sites, a theory supported by studies of barnase (Arcus et al., 1995; Freund et al., 1996) and barstar (Wong et al., 1996).

Unfortunately, motions on the ms to μs timescale are difficult to measure. The classical trio of R_1, R_2 and heteronuclear NOE experiments can be used to map motions that are faster than the overall correlation time only, although chemical exchange may affect the results. The Lipari–Szabo 'model-free' approach is often used to estimate exchange contributions from these parameters (Lipari and Szabo, 1982a, b), but does not include sufficient information to predict explicit rates and dispersion amplitudes (a function of the chemical shift difference and populations of exchanging species). Furthermore, because exchange contributions, R_{ex}, are determined essentially as deviations from averaged R_2 rates, they may be significantly biased by anisotropic rotational diffusion (Tjandra et al., 1995). The dependence of transverse relaxation on static field strength (Phan et al., 1996; Vis et al., 1998) provides a direct measure of R_{ex}. Even more powerful, a new application for the measurement of ^{1}H-^{15}N dipolar/^{15}N CSA cross-correlation rates provides a useful way to distinguish the effects of chemical exchange and anisotropy (Kroenke et al., 1998). To characterize explicit rates of exchange, R_2 is monitored as a function of CPMG refocusing delay length (Allerhand and Gutowsky, 1965; Orekhov et al., 1994), spin lock field strength (Deverell et al., 1970; Szyperski et al., 1993; Akke and Palmer, 1996), or temperature (Mandel et al., 1996). However, each of these techniques is limited to a certain range of timescales. Quantification of a chemical exchange process is most accurate when the timescale of the process is within the limits imposed by the technique, and the dispersion amplitude is significant.

The third fibronectin type III domain from human tenascin, TNfn3$_{1-90}$, a β sandwich immunoglobulin-like domain, provides an excellent model system for an in-depth study of transverse relaxation. Chemical exchange exists on a wide range of timescales (Akke et al., 1998; Meekhof et al., 1998), and significant rotational anisotropy is suggested by the ratio of its principle moments of inertia: $1.0 \times 0.9 \times 0.41$ (Leahy et al., 1992). By combining the results of T_2-CPMG and off-resonance $T_{1\rho}$ experiments, we report transverse relaxation rates for backbone ^{15}N nuclei over an exceptionally wide range of effective field strengths (2–40 krad/s). Slow chemical exchange observed for several residues surrounding the C terminus is fully characterized; faster exchange events for five residues scattered throughout the domain ($\tau_{ex} < 50$ μs) could not be measured. The acquisition of 16 independent transverse relaxation rates for most ^{15}N nuclei allows us to define and discuss the intrinsic uncertainty in measuring R_2. R_1 and averaged exchange-free R_2 values, R_2^0, are used to calculate diffusion tensors for isotropic, axially symmetric, and fully anisotropic models. Interestingly, constraining the input set to residues in defined secondary structure leads to a prediction of isotropic diffusion. Loop residues, whose N-H vectors exhibit a wider range of tilt angles (θ_{N-H}) to the major diffusion axis, are instrumental for defining the rotational anisotropy.

Materials and methods

Sample preparation

TNfn3$_{1-90}$, a fibronectin type III domain corresponding to residues 802–891 of human tenascin-C, was expressed and purified according to procedures described by Clarke et al. (1997). Uniformly ^{15}N-labeled samples were obtained through bacterial growth in M9 minimal media using ^{15}N-labeled ammonium chloride as the sole nitrogen source. NMR samples were 1.0 mM in protein, and contained 50 mM deuterated acetate buffer, pH 4.9, in 90% H_2O/10% D_2O. The total volume of each sample was 0.5 mL.

NMR spectroscopy

NMR experiments were collected on a Bruker DRX 600 spectrometer (operating at 600.13 MHz ^{1}H frequency) equipped with an inverse detection triple resonance probe and triple axis gradients. Experiments were performed at 300 K and incorporated gradient selection for water suppression and sensitivity enhancement (Kay et al., 1992). Sequence-specific assignments were presented in a previous publication (Meekhof et al., 1998).

To monitor transverse relaxation under relatively weak effective B_1 fields, relaxation rates, R_2, of backbone ^{15}N nuclei were measured as a function of the spin-echo delay in T_2-CPMG experiments (Bloom et al., 1965; Orekhov et al., 1994). Sets of experiments were collected at six CPMG refocusing delays (τ): 311, 498, 686, 900, 1061 and 1436 μs. The effective field strength, ω_{eff}, of the CPMG pulse train at each of these delays was calculated as the rate at which ^{15}N magnetization is rotated through 360°:

$$\omega_{eff}\,(\mathrm{rad/s}) = 2\pi\left(\frac{1}{2(\mathrm{T}_\pi + \tau)}\right) \qquad (1)$$

T_π is the duration of a 180°^{15}N CPMG pulse (78 μs). The suppression of relaxation due to chemical exchange (R_{ex}) occurs when the frequency of the exchange process is similar to, or slower than, the frequency of refocusing pulses. When the pulse repetition rate is significantly faster than the exchange rate, R_{ex} contributions are completely suppressed. Alternatively, if the shortest refocusing delay has no effect on reducing R_{ex}, then the rate of exchange must be at least $3.2/\tau$. Experimental limits on the spin-echo delay length are determined by the duty cycle of the transmitter for short delays and the evolution of ^{1}H-^{15}N coupling during long delays. Here, these limits provide access to effective fields between 2 and 8 krad/s. At each refocusing delay, a series of 12 experiments with relaxation times ranging from 6 to 180 ms was obtained. These experiments were collected in randomized order, with respect to both refocusing delay and mixing time, in order to minimize systematic errors. In all cases, the recycle delay was 3.0 s. The acquisition time for each experiment was 2 h, for a total of 24 h per data set.

The effects of stronger spin-lock fields on transverse relaxation were monitored in off-resonance $T_{1\rho}$ experiments (Akke and Palmer, 1996; Zinn-Justin et al., 1997; Banci et al., 1998). In contrast to the on-resonance approach (Deverell et al., 1970), for which ω_{eff} depends upon the strength of the transverse spin-lock field (B_1), the B_1 offset (Δ) is incremented to yield a variable ω_{eff} as the vector product of B_1 and Δ:

$$\omega_{eff}\,(\mathrm{rad/s}) = 2\pi\sqrt{B_1^2 + \Delta^2} \qquad (2)$$

The angle determined by Δ and ω_{eff} in the rotating frame is the tilt angle, θ. Although applied fields (B_1) are of moderate strength, harnessing the power of the static field provides access to effective fields of up to 40 krad/s. Sampling exchange frequencies at such fast timescales is not possible with other established methods.

Alignment of the off-resonance spin-lock was attained by adiabatic rotation of the nuclear spin magnetization via simultaneous hyperbolic tangent amplitude and tangent frequency modulated rf pulses over a 4 ms period (Mulder et al., 1998). By applying a transverse (B_1) spin-lock field of 1.8 kHz and varying the frequency offset (measured to the center of the amide spectrum) from 0 to -5836 Hz in sets of experiments, $R_{1\rho}$ relaxation rates were measured at 10 tilt angles, θ, between 17° and 90°. At each offset, a series of eight experiments with mixing times of 30 to 400 ms was collected. The recycle delay was 2.0 s, and the uncertainty in B_1, estimated from calibration of a 360° ^{15}N pulse, was $\pm$ 3%. Experiments were collected in randomized order. The time required for each experiment was 1 h, for a total of 80 h for the entire data set. The excitation profile at each field offset was verified in a series of 1D spectra obtained for a glycine test sample.

^{15}N longitudinal relaxation rates, R_1, were measured with standard inversion-recovery experiments (Kay et al., 1989). Relaxation delays were set to 40, 200, 300, 400, 500, 600, 800 and 1000 ms, and the recycle delay was 2.0 s.

2D ^{1}H-^{15}N correlation spectra of 1024×256 points each were collected for all experiments described above. Spectral widths were generally 9615 Hz in the ^{1}H dimension and 2000 Hz in the ^{15}N dimension. Spectra were processed and analyzed using Felix 2.30 (Biosym). For each set of experiments, maximum cross peak intensities were plotted against the mixing time and fit to two-parameter exponential decay curves in Kaleidagraph (Abelbeck software) to determine ^{15}N relaxation rates and uncertainties for individual amides.

Extracting transverse relaxation rates from the off-resonance $T_{1\rho}$ *experiment*

Relaxation in the rotating frame, $R_{1\rho}$, depends upon the tilt angle, θ, between ω_{eff} and the z-axis (B_0), and the corresponding rates of longitudinal and transverse relaxation, R_1 and R_2 (Davis et al., 1994; Akke and Palmer, 1996):

$$R_{1\rho} = R_1 \cos^2\theta + R_2 \sin^2\theta \qquad (3)$$

Although R_2 is nominally restricted to the effects of dipole-dipole interactions and chemical shift anisotropy, chemical exchange on a ms to μs timescale can augment transverse relaxation rates by providing an alternate relaxation mechanism.

After calibrating the set of ^{15}N offsets for each residue, plots of $R_{1\rho}$ versus θ were constructed (Zinn-Justin et al., 1997). Independently acquired values for R_1 and R_2 (from the T_2-CPMG experiment, where τ = 900 μs) were added to each plot at θ = 0° and θ = 90°, respectively, and were compared to values determined from the optimized fitting of all 12 points (Figure 1). In the absence of chemical exchange, there was good agreement.

Using independently acquired R_1 values, the transverse relaxation component of $R_{1\rho}$ for each residue at each offset angle, R_2(calc), was determined (Equation 3). Each value of R_2(calc) includes contributions from chemical shift anisotropy, dipole-dipole coupling, and, if present, chemical exchange. Propagated uncertainties in R_2(calc) incorporate uncertainties in both $R_{1\rho}$ and the strength of the spin-lock field, and increase dramatically with ω_{eff}.

Calculating rates of chemical exchange

Knowing the effective field strength of a CPMG pulse train (Equation 1) allows R_2 rates measured in T_2-CPMG experiments to be compared with values of R_2(calc) extracted from $T_{1\rho}$ data sets. Transverse relaxation rates from both experiments were combined and plotted against ω_{eff}. For each residue, variations in R_2 were used to calculate chemical exchange time constants, τ_{ex}, defined as $(k_{A\rightarrow B} + k_{B\rightarrow A})^{-1}$, from optimized fits to the following equation (Akke and Palmer, 1996):

$$R_2,\, R_2(calc) = R_2^0 + \frac{(\delta\omega)^2 p_A p_B \tau_{ex}}{(1 + \omega_{eff}^2 \tau_{ex}^2)} \qquad (4)$$

R_2^0 is the 'exchange free' transverse relaxation rate; the second term represents the exchange contribution, R_{ex}. Exchange is assumed to occur between two populations, p_A and p_B, with a chemical shift difference of δω. To be observed, the transition must have significant amplitude (δω > 0). Tracking transverse relaxation over such a wide range of effective fields (2–40 krad/s) allows rates of chemical exchange over a broad ms to μs timescale to be measured with confidence.

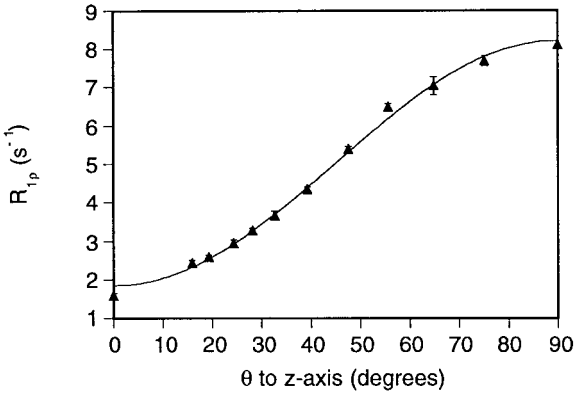

Figure 1. Off-resonance $R_{1\rho}$ relaxation rates for Asp 78 at 300 K are plotted against the tilt angle, θ, between the z-axis and the effective field. Independently measured R_1 and R_2 (T_2-CPMG) relaxation rates are indicated at θ = 0° and θ = 90°, respectively. The relationship among R_1, R_2 and $R_{1\rho}$ is indicated by the optimized curve fit of Equation 3 to all 12 data points.

Diffusion anisotropy calculations

Diffusion tensors for isotropic, axially symmetric, and anisotropic models were determined at 300 K using the local diffusion approach (Brüschweiler et al., 1995; Lee et al., 1997). Local diffusion constants are calculated for each N-H bond vector from R_2^0/R_1 ratios, and are used to construct the overall diffusion tensor. The diffusion tensor is defined by up to six independent variables. D_{zz}, D_{yy} and D_{xx} represent its principal components, where $D_{zz} > D_{yy} > D_{xx}$. The polar angles θ and φ define the orientation of D_{zz} with respect to the coordinate system of the original

PDB file (1ten), and Ψ, the orientation of D_{xx}. In the case of axially symmetric diffusion, $D_{par} = D_{zz}$ and $D_{per} = (D_{xx} + D_{yy})/2$. $D_{xx} = D_{yy}$, and Ψ is not required (Tjandra et al., 1995). By convention, residues experiencing significant high mobility motion (with a heteronuclear NOE < 0.65) or with chemical exchange (here, residues for which R_2^0 was not determined) were excluded from the analysis, leaving a total of 59 data points. The X-ray crystal structure of $TNfn3_{1-90}$ was used to define the relative orientations of all N-H vectors (Leahy et al., 1992). The 'goodness of fit' for each model was determined by the χ^2 statistic. Fits were compared by the statistical *F*-test, which indicates whether or not χ^2 is improved solely because of an increased number of fitting parameters (Bevington and Robinson, 1992; Tjandra et al., 1996; Lee et al., 1997).

Results

Measuring R_2 *in the presence of a CPMG spin-echo pulse train*

Transverse relaxation rates were measured for 71 of the 85 non-proline residues in $TNfn3_{1-90}$ at six effective fields between 2 and 8 krad/s. By plotting R_2 against ω_{eff} (Equation 4), three categories of residues were identified. In the largest set, R_2 does not vary with ω_{eff} and is roughly equivalent for all residues. The aggregate average, $7.22 \pm 0.49\ s^{-1}$, is consistent with the intrinsic value predicted for a protein of this size (approximately 10 kDa). In the second set, comprising residues 40, 45, 52, 55 and 68, R_2 does not vary with ω_{eff} but is significantly elevated, suggesting the presence of chemical exchange on faster timescales. For the remaining residues – 10, 17, 20, 63, 87 and 90 – chemical exchange occurs on the timescale of the CPMG experiment, with an average time constant of 568 μs and a standard deviation of only 32 μs. These residues are all located within 12 Å of the C terminus, and were shown in a previous report (Meekhof et al., 1998) to engage in concerted fluctuations resulting from premature domain truncation. In that report, a detailed characterization of their exchange parameters is provided.

Measuring R_2 *via off-resonance* $T_{1\rho}$ *relaxation*

For the same 71 residues, off-resonance $R_{1\rho}$ relaxation monitored at 10 tilt angles, θ, provided insight into transverse relaxation rates under effective fields of 10 to 40 krad/s. For residues lacking chemical exchange, and for those with chemical exchange on the timescale of the CPMG experiment, a constant R_2(calc) similar to the base rate observed in the CPMG experiments was observed across the range of field strengths. The cumulative average was $7.27 \pm 0.69\ s^{-1}$. For residues exhibiting invariant but elevated R_2 relaxation rates in the CPMG experiment (40, 45, 52, 55 and 68), extracted R_2(calc) values were similarly independent of ω_{eff}. These residues appear to undergo fast chemical exchange on a timescale outside the boundaries of the experiment ($\tau_{ex} < 50$ μs), a hypothesis confirmed by line broadening of approximately 1–4 Hz along the ^{15}N axis for all five residues. A direct correspondence exists between the degree of line broadening and the magnitude of explicitly measured exchange contribution (R_{ex}), despite the fact that the digital resolution in the ^{15}N dimension is only 2.4 Hz/point after twofold zero filling.

In the off-resonance experiment, transverse relaxation rates are obtained indirectly, and there are a few limitations to our approach. Extracted values of R_2(calc) are heavily dependent on the value of R_1 used in Equation 3. By modeling the effects of artificially increased, or decreased, input R_1 values, we were able to simulate the impression of a chemical exchange process for individual residues. Secondly, as the tilt angle, θ, between the effective magnetization and the z-axis decreases, the contribution of R_2 to $R_{1\rho}$ diminishes (Equation 3), and extracted transverse relaxation rates contain a sizable uncertainty. Values of R_2(calc) determined for several of the furthest off-resonance points ($\theta < 33°$) were often more than one standard deviation from the aggregate mean; these were omitted from further analysis. At the opposite limit of the offset range, we observed that $R_{1\rho}$ relaxation rates for residues upfield, or up to 150 Hz downfield, of the applied B_1 field were often slower than expected. This behavior was replicated in tests on a glycine sample and may result from limitations in the homogeneity of the B_1 field. These points were also discluded from further analysis. $R_{1\rho}$ relaxation rates measured at offset tilt angles between 30° and 80° are the most reliable.

Comparing the results of T_2*-CPMG and* $T_{1\rho}$ *experiments*

To ensure that there was no systematic difference between the CPMG and $T_{1\rho}$ experiments, we compared, for each residue, the average R_2 obtained from the six CPMG experiments with the average R_2(calc) ob-

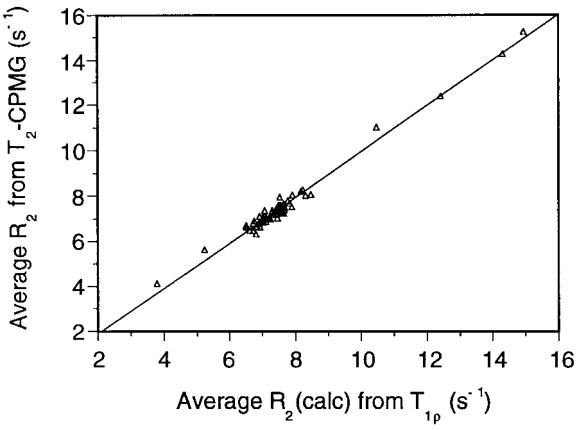

Figure 2. Average transverse relaxation rates determined by T_2-CPMG (6 experiments per point) and off-resonance $T_{1\rho}$ experiments (10 experiments per point) are compared. Residues with measured chemical exchange events (10, 17, 20, 63, 87, 90) have been excluded. A linear correlation yields a slope of 1.01, with a y-intercept of -0.12 and a correlation coefficient of 0.99. Such agreement confirms that results of the two methods can be directly compared, and establishes the accuracy of the reported rates. For the four residues with R_2 greater than 10 s^{-1}, chemical exchange ($\tau_{ex} < 50$ μs timescale) occurs outside the detection limit.

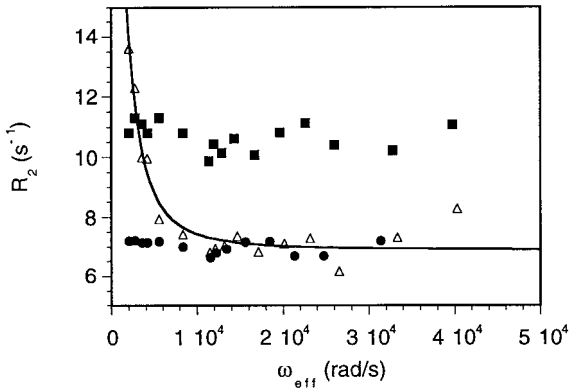

Figure 3. Transverse relaxation rates are plotted against effective field strength, ω_{eff}, for three residues in TNfn3$_{1-90}$. Points between 2 and 10 krad/s are obtained by T_2-CPMG experiments, and between 10 and 40 krad/s by the off-resonance $T_{1\rho}$ approach. For Ile 8 (filled circles), the assigned exchange-free transverse relaxation rate, R_2^0, represents the average of all data points. For Val 10 (open triangles), chemical exchange on slow timescales affects R_2 at the lowest field strengths only; R_2^0 is obtained from extrapolation of the curve (Equation 4) to infinite field strength. For Arg 45 (filled squares), elevated rates of relaxation result from chemical exchange on a timescale < 50 μs. Variations in R_2 reflect the uncertainty of the experiment, and R_2^0 cannot be obtained. Error bars have been omitted for clarity, but increase with ω_{eff}.

tained from the $T_{1\rho}$ data set (Figure 2). Comparisons were omitted for the six residues with observed chemical exchange events. The points determine a line with a slope of 1.01, y-intercept of -0.12, and correlation coefficient of 0.99, demonstrating that results of the two methods may be directly compared (Zinn-Justin et al., 1997). Combined plots of R_2 and R_2(calc) versus effective field strength were constructed for all residues; a few are presented in Figure 3. Although averaged rates from the CPMG and $T_{1\rho}$ experiments are similar, Figure 3 illustrates the variation in isolated measurements. The average and standard deviations of all R_2 rates obtained for each residue are available from the authors as supplementary material.

Determining parameters for diffusion anisotropy

For a given ^{15}N nucleus, the ratio between R_2^0 and R_1 is approximately unaffected by rapid internal motions and the magnitude of the CSA tensor, and provides a reliable basis for calculating the effective tumbling time, $\tau_{c,eff}$ of N-H bond vectors. For an isotropically tumbling protein, $\tau_{c,eff}$ is constant along the protein sequence. When diffusion is not isotropic, $\tau_{c,eff}$ varies with θ_{N-H}. If not explicitly considered in motional models, anisotropy may be mistakenly interpreted as slow internal motion on the ns timescale, or chemical exchange on the ms to μs timescale, or may simply prevent adequate fitting of the model to the experimen-

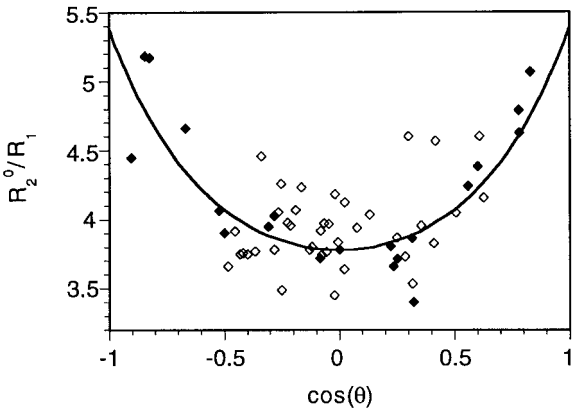

Figure 4. The ratio of R_2^0 and R_1 for residues in TNfn3$_{1-90}$ is plotted against cos(θ_{N-H}), where θ_{N-H} is the angle separating the unique diffusion axis of the protein (axially symmetric model) from individual N-H vectors. The solid line indicates the theoretical prediction for a protein with a τ_c of 5.7 ns and a D_{par}/D_{per} of 1.55. Rotational anisotropy is defined primarily by residues in the loop regions (filled diamonds), as the majority of residues within the β sandwich (open diamonds) are roughly perpendicular to the unique diffusion axis. In fact, the β sheet residues (BETA set) can be sufficiently described by isotropic diffusion (Table 1).

tal data (Schurr et al., 1994; Phan et al., 1996; Tjandra et al., 1996; Luginbühl et al., 1997; Kroenke et al., 1998).

Parameters for isotropic, axially symmetric, and fully anisotropic diffusion models were calculated in two complementary approaches. In the first, averaged R_2^0 values were used as inputs, and the results are presented in Table 1. The TNfn3$_{1-90}$ data are best described by an axially symmetric diffusion tensor with a $\tau_{c,eff}$ of 5.73 ns and D_{par}/D_{per} of 1.55. The reduced χ^2 (χ^2_{red}) is 1.55. With a χ^2_{red} of 1.43 ($F = 2.96$), the fully anisotropic model does not represent a significant improvement.

In order to gauge the impact of experimental variability in R_2, diffusion parameters were also calculated from the separate sets of R_2 rates obtained at each effective field strength. The axially symmetric diffusion model was favored in all calculations, but consensus among the other parameters was less evident. For the axially symmetric model, estimates for τ_c ranged from 5.46 to 5.85, with an average of 5.70. The ratio of D_{par}/D_{per} ranged from 1.25 to 1.52, with an average of 1.39. The orientations of the diffusion axes were generally within $\pm 20°$ of the angles reported in Table 1. Values for χ^2_{red} ranged between 2.02 and 3.45. These variations extend beyond the range of uncertainty predicted by the original calculation, and demonstrate the potential limitations of using a single set of R_2 data points to construct diffusion models.

According to one convention, the diffusion tensor should be assigned only on the basis of relaxation data for residues in fixed elements of secondary structure (Gagné et al., 1998). The rationale for this approach is that in flexible loop regions, N-H vectors may not orient along a fixed angle to the major diffusion axis. To test this approach, new models for all three diffusion tensors were constructed using data (averaged R_2^0 values) for residues in the β sheets of TNfn3$_{1-90}$ only. Strikingly, the model for simple isotropic diffusion ($\tau_{c,eff} = 5.40$ ns) is sufficient ($\chi^2_{red} = 1.54$), and results from the fact that N-H vectors within a β sheet have a similar orientation, and do not exhibit a wide range of θ_{N-H} angles with respect to any diffusion axis.

In Figure 4, averaged R_2^0/R_1 ratios for residues in the β sheet and loop regions are distinguished and plotted against θ_{N-H}. The greater dispersion of θ_{N-H} angles within the loops is illustrated. The solid line indicates the theoretical ratio for a protein with $\tau_c = 5.7$ and $D_{par}/D_{per} = 1.55$, and is calculated from the spectral density function (Farrow et al., 1995) as defined by the axially symmetric model free formalism (Kroenke et al., 1998). Values of $\cos(\theta_{N-H})$ for individual residues are available as supplementary material. In Figure 5, the structure of TNfn3$_{1-90}$ is aligned with the principal axes of the axially symmetric diffusion tensor. The major axis, z, is parallel to the β sandwich.

Discussion

The explicit measurement of chemical exchange on the ms to μs timescale has two advantages. From a practical perspective, exchange often corresponds to biologically important events such as molecular recognition, ligand binding, and catalysis, for which rate information is useful. On a more fundamental level, subtracting the effects of exchange from transverse relaxation rates provides access to R_2^0, the 'exchange free' transverse relaxation rate. It is this parameter that is properly used to define the spectral density function, $J(\omega)$, the foundation of all motional models.

Figure 6 demonstrates the need for measuring R_2 over a wide range of effective fields when chemical exchange on a variety of timescales is expected. It also illustrates the increasing difficulty of measuring fast exchange events, particularly when the amplitude of the event ($\Delta\omega$) is not large. Although normally applied in isolation, T_2-CPMG and off-resonance $T_{1\rho}$ experiments can be combined to provide an unbroken spectrum of R_2 data points, and characterization of exchange events on the ms to μs timescale (Davis et al., 1994). For TNfn3$_{1-90}$, collective exchange motions with a time constant of approximately 568 μs were characterized for a cluster of residues surrounding the C terminus (Meekhof et al., 1998). Rates for exchange events on a timescale faster than 50 μs could not be obtained. An increased uncertainty in calculating fast rates of exchange is unavoidable, since the contribution of chemical exchange to relaxation in the rotating frame decreases with θ.

One significant outcome of collecting such a large number (16) of transverse relaxation rates for each ^{15}N nucleus is that the intrinsic uncertainty in measuring R_2^0 can be learned. Here, the aggregate average of R_2^0 for each residue is based not on replicate measurements under similar conditions, but on a series of measurements at different effective field strengths. Even in the absence of exchange, recorded rates exhibit random scattering with a median standard deviation of 0.31 (within a range of 0.09 to 0.72). For assigning

Table 1. Calculated diffusion parameters for $TNfn3_{1-90}$[a]

Data set	Model	$\tau_{c,eff}$ (ns)[b]	$2D_{zx}/(D_{xx}+D_{yy})$	D_{xx}/D_{yy}	θ (deg)	φ (deg)	Ψ (deg)	χ^2_{red}[c]	F[d]
$TNfn3_{1-90}$	Isotropic	5.50	1	1				3.11	
	Ax symm.	5.73	1.55	1	78	91		1.55	20.40
	Asymm.	5.73	1.55	1.17	92	−29	26	1.43	2.96
$TNfn3_{1-90}$	Isotropic	5.40	1	1				1.54	
(BETA)[e]	Ax symm.	5.39	1.06	1	84	−77		1.55	0.96
	Asymm.	5.50	1.30	1.12	91	19	19	1.61	0.31

[a]Diffusion tensors were calculated from the averaged R_2^0/R_1 ratios of individual ^{15}N nuclei at 300 K according to the local diffusion method. Structure coordinates were taken from the X-ray crystal structure (PDB entry 1ten).

[b]$\tau_{c,eff}$ was calculated as $(6D_{iso})^{-1}$, where $D_{iso} = (D_{par} + 2D_{per})/3 = (D_{xx} + D_{yy} + D_{zz})/3$.

[c]The 'goodness of fit' parameter, χ^2, is normalized by the number of degrees of freedom (number of residues minus number of fitted parameters) to yield χ^2_{red}.

[d]The *F*-statistic compares the isotropic to the axially symmetric model, and the axially symmetric to the fully anisotropic model, for each data set.

[e]The $TNfn3_{1-90}$ BETA set includes only the residues comprising the β sandwich.

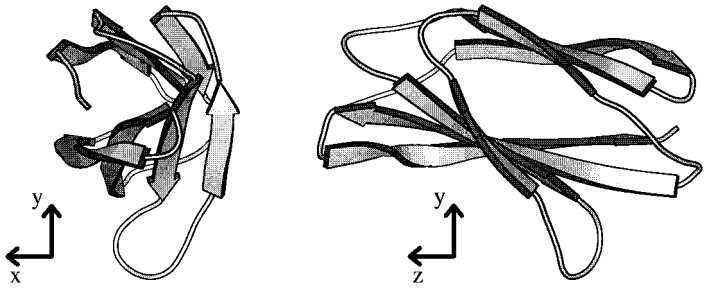

Figure 5. $TNfn3_{1-90}$ is shown with its major diffusion axis (rotated to the z-axis) aligned perpendicular to, and parallel to, the plane of the page. The domain exhibits axially symmetric anisotropic diffusion with a D_{par}/D_{per} of 1.55 ± 0.08. N-H vectors within the β sandwich are roughly parallel, and do not themselves permit identification of the diffusion anisotropy. The twist in one of the strands is caused by a β bulge at Pro 83.

true R_2^0 values, an average established by several measurements of R_2 may be significantly more reliable than a single data point. An improved certainty in the measurement of all relaxation parameters is important for the construction of motional models (Jin et al., 1997) and the characterization of diffusion anisotropy, as shown in this report.

'Exchange free' transverse relaxation rates, R_2^0, are directly related to the spectral density function, and can be used in combination with R_1 rates and ^{15}N-$\{^1H\}$ NOE enhancements to characterize molecular mobility and construct the overall diffusion tensor (Lipari and Szabo, 1982a,b). A qualitative assessment of the motional properties of $TNfn3_{1-90}$ was obtained by plotting the averaged T_2^0 $(1/R_2^0)$ versus T_1 $(1/R_1)$ for each amide ^{15}N nucleus in the domain (Figure 7). The plot was overlaid with theoretical curves, derived from the Lipari–Szabo model-free formalism, that trace the dependence of the isotropic correlation time, $\tau_{c,eff}$, on

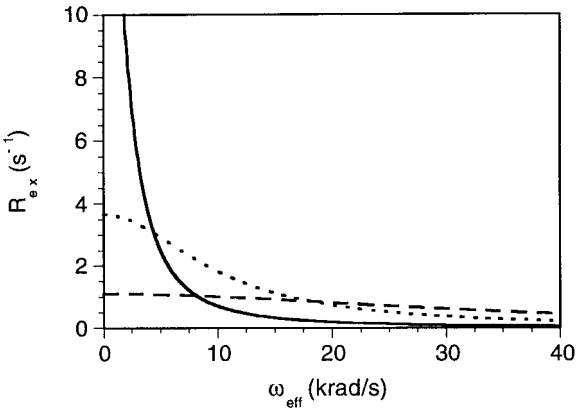

Figure 6. The contribution (in Hz) of chemical exchange to observed transverse relaxation rates is simulated for processes occurring at 500 μs (solid line), 100 μs (dotted line), and 30 μs (dashed line). In all cases, the Δδ between exchanging species is 60 Hz, with $p_A = p_B = 0.5$. The range of effective fields matches those sampled in the reported results. To be accurately measured, an exchange process must have sufficient amplitude (Δω), and occur within the recorded range of timescales.

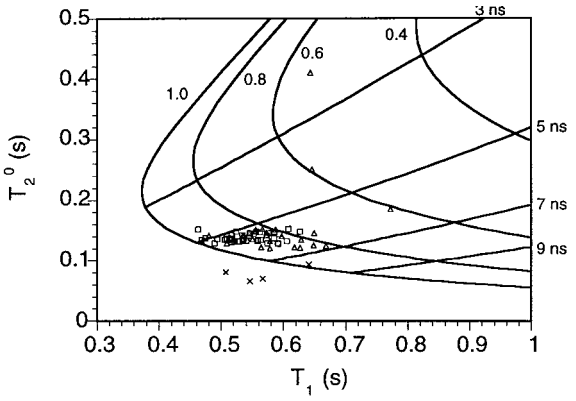

Figure 7. Backbone ^{15}N R_2^0 and R_1 relaxation rates for TNfn3$_{1-90}$ are plotted as their reciprocals, T_2^0 and T_1. Each point corresponds to a single amino acid residue. Residues in β structure are indicated by squares, those in loop regions by triangles, and those with unaccounted chemical exchange contributions by crosses. Overlaid on the plot, contours indicate the relationship between T_1, T_2^0, the generalized model-free order parameter S^2, and the effective correlation time $\tau_{c,eff}$. (To construct the plot, the correlation time for internal motions, τ_e, was fixed at 50 ps. This assignment affects the apparent clustering of the points – increasing τ_e would decrease predicted values of S^2.) Curved lines demonstrate the variation in $\tau_{c,eff}$ for fixed values of S^2, while straight lines indicate the reverse. All residues fall within the allowed $S^2 = 1$ boundary, except those with non-measurable exchange contributions. Because the domain is dominated by a single secondary structural element with roughly parallel N-H vectors, most points fall within a single cluster. Residues within the loops exhibit some of the longest correlation times, in accordance with the alignment of their N-H vectors along the major diffusion axis.

S^2, the model-free order parameter, and vice versa. With τ_e fixed at 50 ps, the bulk of residues comprise a single cluster between $S^2 = 0.8$ and $S^2 = 1$, with an average $\tau_{c,eff}$ of 5.50, the effective correlation time determined by the isotropic diffusion model (Table 1). Significant variations in T_1 forecast the presence of anisotropic diffusion. For this 10 kDa protein, T_1 is a far more sensitive parameter than T_2^0 to variations in effective correlation time (Broadhurst et al., 1995). Loop residues, many of which have N-H bond vectors nearly parallel to the major diffusion axis, exhibit the largest $\tau_{c,eff}$ values. Only residues exhibiting unaccounted chemical exchange (fast μs timescale) fall outside of the allowed $S^2 = 1$ boundary; this is a result of alternative transverse relaxation mechanisms.

The asymmetric moments of inertia of the TNfn3$_{1-90}$ domain, $1.0 \times 0.9 \times 0.41$, forecast a significant degree of rotational anisotropy (Leahy et al., 1992). However, an accurate characterization of this effect is hindered by a narrow dispersion of tilt angles, θ_{N-H}, between amide N-H vectors in the β sheet and the major diffusion axis, an intrinsic problem for many proteins (Lee et al., 1997). Residues in loops exhibit a wider dispersion of θ_{N-H} angles and are required to define the rotational anisotropy, presenting a three-part challenge. First, the defined orientations of residues in loop regions are the most likely ones to be affected by crystal packing. Second, increased flexibility decreases certainty in θ_{N-H} – the relationship between the range of orientations experienced by loop N-H vectors in solution and the orientation adopted in the crystal structure is unknown. Lastly, the paucity of residues with $\cos(\theta) > 0.5$ prevents a robust definition of the diffusion tensor.

Conclusions

By measuring rates of chemical exchange, and calculating the diffusion anisotropy, we have accounted for many of the variations in ^{15}N R_1 and R_2 relaxation rates along the TNfn3$_{1-90}$ backbone. Results of T_2-CPMG and off-resonance $T_{1\rho}$ experiments were successfully combined to provide transverse relaxation rates over a continuous and broad range of effective field strengths. Acquiring 16 independent rates for each ^{15}N nucleus also revealed the intrinsic uncertainty in measuring R_2. The median standard deviation of rates obtained for non-exchanging residues was 0.31, suggesting that an average obtained from a series of measurements may provide a more accurate valuation of the 'true' R_2^0.

Acknowledgements

We thank Alan Fersht for providing facilities and support. Discussions with Rolf Boelens, Frans Mulder, and Mark Howard are gratefully acknowledged. We thank the referees for their insightful comments, and Arthur Palmer for providing diffusion analysis programs on his website. A.E.M. is supported by a National Science Foundation Graduate Fellowship.

References

Akke, M., Liu, J., Cavanagh, J., Erickson, H.P. and Palmer, A.G. (1998) *Nat. Struct. Biol.*, **5**, 55–59.

Akke, M. and Palmer, A.G. (1996) *J. Am. Chem. Soc.*, **118**, 911–912.

Allerhand, A. and Gutowsky, H.S. (1965) *J. Chem. Phys.*, **42**, 1587–1599.

Arcus, V.A., Vuilleumier, S., Freund, S.M.V., Bycroft, M. and Fersht, A.R. (1995) *J. Mol. Biol.*, **254**, 305–321.

Banci, L., Bertini, I., Cavazza, C., Felli, I.C. and Koulougliotis, D. (1998) *Biochemistry*, **37**, 12320–12330.

Bevington, P.R. and Robinson, D.K. (1992) *Data Reduction and Error Analysis for the Physical Sciences* (2nd ed.), McGraw-Hill, New York, NY.

Bloom, M., Reeves, L.W. and Wells, E.J. (1965) *J. Chem. Phys.*, **42**, 1615–1624.

Broadhurst, R.W., Hardman, C.H., Thomas, J.O. and Laue, E.D. (1995) *Biochemistry*, **34**, 16608–16617.

Brüschweiler, R., Liao, X. and Wright, P.E. (1995) *Science*, **268**, 886–888.

Carr, H.Y. and Purcell, E.M. (1954) *Phys. Rev.*, **94**, 630–638.

Clarke, J., Hamill, S.J. and Johnson, C.M. (1997) *J. Mol. Biol.*, **270**, 771–778.

Constantine, K.L., Friedrichs, M.S., Wittekind, M., Jamil, H., Chu, C.-H., Parker, R.A., Goldfarb, V., Mueller, L. and Farmer, B.T. (1998) *Biochemistry*, **37**, 7965–7980.

Davis, D.G., Perlman, M.E. and London, R.E. (1994) *J. Magn. Reson.*, **B104**, 266–275.

Deverell, C., Morgan, R.E. and Strange, J.H. (1970) *Mol. Phys.*, **18**, 552–559.

Farrow, N.A., Zhang, O., Szabo, D., Torchia, D.A. and Kay, L.E. (1995) *J. Biomol. NMR*, **6**, 153–162.

Freund, S.M.V., Wong, K.-B. and Fersht, A.R. (1996) *Proc. Natl. Acad. Sci. USA*, **93**, 10600–10603.

Gagné, S.M., Tsuda, S., Spyracopoulos, L., Kay, L.E. and Sykes, B.D. (1998) *J. Mol. Biol.*, **278**, 667–686.

Jin, D., Figueirido, F., Montelione, G.T. and Levy, R.M. (1997) *J. Am. Chem. Soc.*, **119**, 6923–6924.

Kay, L.E. (1998) *Nat. Struct. Biol.*, **5**, 513–517.

Kay, L.E., Keifer, P. and Saarinen, T. (1992) *J. Am. Chem. Soc.*, **114**, 10663–10665.

Kay, L.E., Torchia, D.A. and Bax, A. (1989) *Biochemistry*, **28**, 8972–8979.

Kroenke, C.D., Loria, J.P., Lee, L.K., Rance, M. and Palmer, A.G. (1998) *J. Am. Chem. Soc.*, **120**, 7905–7915.

Lane, A.N. and Lefévre, J.-F. (1994) *Methods Enzymol.*, **239**, 596–619.

Leahy, D.J., Hendrickson, W.A., Aukhil, I. and Erickson, H.A. (1992) *Science*, **258**, 987–991.

Lee, L.K., Rance, M., Chazin, W.J. and Palmer, A.G. (1997) *J. Biomol. NMR*, **9**, 287–298.

Lipari, G. and Szabo, A. (1982a) *J. Am. Chem. Soc.*, **104**, 4546–4559.

Lipari, G. and Szabo, A. (1982b) *J. Am. Chem. Soc.*, **104**, 4559–4570.

Luginbühl, P., Pervushin, K.V., Iwai, H. and Wüthrich, K. (1997) *Biochemistry*, **36**, 7305–7312.

Mandel, A.M., Akke, M. and Palmer, A.G. (1996) *Biochemistry*, **35**, 16009–16023.

McIntosh, P.B., Frenkiel, T.A., Wollborn, U., McCormick, J.E., Klempnauer, K.H., Feeney, J. and Carr, M.D. (1998) *Biochemistry*, **37**, 9619–9629.

Meekhof, A.E., Hamill, S.J., Arcus, V.L., Clarke, J. and Freund, S.M.V. (1998) *J. Mol. Biol.*, **282**, 181–194.

Mulder, F.A.A., de Graff, R.A., Kaptein, R. and Boelens, R. (1998) *J. Magn. Reson.*, **131**, 351–357.

Ogata, K., Kanei-Ishii, C., Sasaki, M., Hatanaka, H., Nagadoi, A., Enari, M., Nakamura, H., Nishimura, Y., Ishii, S. and Aarai, A. (1996) *Nat. Struct. Biol.*, **3**, 178–187.

Orekhov, V.Y., Pervushin, K.V. and Arseniev, A.S. (1994) *Eur. J. Biochem.*, **219**, 887–896.

Palmer, A.G. (1997) *Curr. Opin. Struct. Biol.*, **7**, 732–737.

Pervushin, K., Riek, R., Wider, G. and Wüthrich, K. (1997) *Proc. Natl. Acad. Sci. USA*, **94**, 12366–12371.

Phan, I.Q.H., Boyd, J. and Campbell, I.A. (1996) *J. Biomol. NMR*, **8**, 369–378.

Schurr, J.M., Babcock, H.P. and Fujimoto, B.S. (1994) *J. Magn. Reson.*, **B105**, 211–224.

Szyperski, T., Luginbühl, P., Otting, G., Güntert, P. and Wüthrich, K. (1993) *J. Biomol. NMR*, **3**, 151–164.

Tjandra, N., Feller, S.E., Pastor, R.W. and Bax, A. (1995) *J. Am. Chem. Soc.*, **117**, 12562–12566.

Tjandra, N., Wingfield, P., Stahl, S. and Bax, A. (1996) *J. Biomol. NMR*, **8**, 273–284.

Vis, H., Vorgias, C.E., Wilson, K.S., Kaptein, R. and Boelens, R. (1998) *J. Biomol. NMR*, **11**, 265–277.

Whittaker, S.B.M., Boetzel, R., MacDonald, C., Lian, L., Pommer, A.J., Reilly, A., James, R., Kleanthous, C. and Moore, G.R. (1998) *J. Biomol. NMR*, **12**, 145–159.

Wong, K.-B., Freund, S.M.V. and Fersht, A.R. (1996) *J. Mol. Biol.*, **259**, 805–818.

Wyss, D., Dayie, K.T. and Wagner, G. (1997) *Protein Sci.*, **6**, 534–542.

Zinn-Justin, S., Berthault, P., Guenneugues, M. and Desvaux, H. (1997) *J. Biomol. NMR*, **10**, 363–372.